How Does GAP Catalyze the GTPase Reaction of Ras?: A Computer Simulation Study†

Timothy M. Glennon, Jordi Villà, and Arieh Warshel*

Department of Chemistry, University of Southern California, Los Angeles, California 90089-1062

Received March 21, 2000; Revised Manuscript Received May 24, 2000

ABSTRACT: The formation of a complex between p21^{ras} and GAP accelerates the GTPase reaction of p21^{ras} and terminates the signal for cell proliferation. The understanding of this rate acceleration is important for the elucidation of the role of Ras mutants in tumor formation. In principle there are two main options for the origin of the effect of GAP. One is a direct electrostatic interaction between the residues of GAP and the transition state of the Ras-GAP complex and the other is a GAP-induced shift of the structure of Ras to a configuration that increases the stabilization of the transition state. This work examines the relative importance of these options by computer simulations of the catalytic effect of Ras. The simulations use the empirical valence bond (EVB) method to study the GTPase reaction along the alternative associative and dissociative paths. This approach reproduces the trend in the overall experimentally observed catalytic effect of GAP: the calculated effect is 7 ± 3 kcal/mol as compared to the observed effect of ~6.6 kcal/mol. Furthermore, the calculated effect of mutating Arg789 to a nonpolar residue is 3−4 kcal/mol as compared to the observed effect of 4.5 kcal/mol for the Arg789Ala mutation. It is concluded, in agreement with previous proposals, that the effect of Arg789 is associated with its direct interaction with the transition state charge distribution. However, calculations that use the coordinates of Ras from the Ras-GAP complex (referred to here as Ras′) reproduce a significant catalytic effect relative to the Ras coordinates. This indicates that part of the effect of GAP involves a stabilization of a catalytic configuration of Ras. This configuration increases the positive electrostatic potential on the β-phosphate (relative to the corresponding situation in the free Ras). In other words, GAP stabilizes the GDP bound configuration of Ras relative to that of the GTP-bound conformation. The elusive oncogenic effect of mutating Gln61 is also explored. The calculated effect of such mutations in the Ras-GAP complex are found to be small, while the observed effect is very large (8.7 kcal/mol). Since the Ras is locked in its Ras-GAP configuration in our simulations, we conclude that the oncogenic effect of mutation of Gln61 is indirect and is associated most probably with the structural changes of Ras upon forming the Ras-GAP complex. In view of these and the results for the Ras′ we conclude that GAP activates Ras by both direct electrostatic stabilization of the transition state and an indirect allosteric effect that stabilizes the GDP-bound form. The present study also explored the feasibility of the associative and dissociative mechanism in the GTPase reaction of Ras. It is concluded that the reaction is most likely to involve an associative mechanism.

GTP-binding proteins like, for example, p21^{ras} (a protein that plays a central role in signal transduction pathways controlling cell proliferation) can be considered as signal switch molecules that cycle between the GTP-bound ON-state and the GDP-bound OFF-state (*1*). *GTP-binding proteins* are usually switched ON by the action of activated guanine-exchange-factors (GEFs) that catalyze the exchange of protein bound GDP by GTP (*2*). In the GTP-bound ON conformation, these GTP-binding proteins interact specifically with an appropriate effector molecule and thus transmit the corresponding signal to the next downstream component in the signaling cascade(*3*).

All known GTP-binding proteins exhibit a GTPase activity that recycles the protein back to its inactive GDP-bound form. The rate of this reaction is crucial for the corresponding timing of the regulated process: the longer a GTP-binding protein remains in its active GTP-bound state, the longer it will transmit and also amplify a certain signal. Hence, the rate of GTP hydrolysis is of great importance for the right timing of many processes in a cell. It is well-known that mutations that slow the reaction rate biologically activate these signaling proteins leading to an oncogenic Ras-protein that permanently produces a cell growth signal. Mutations at either one of the 12, 13, or 61 positions are found in approximately 30% of human tumors, which is among the highest frequencies of known oncogenes (*4*−*6*).

Very often GTP-binding proteins are regulated and controlled by accessory proteins. For instance, the activation of a GTP-binding protein involves an exchange of bound GDP by GTP and is catalyzed by GEFs. Also, the GTPase activity of GTP-binding proteins is very often controlled by other proteins. The relatively slow intrinsic reaction rate of p21^{ras} (Ras) can be accelerated by up to 5 orders of magnitude in the presence of highly specific GTPase-activating proteins (GAPs) (*7*). GAPs are presumably negative regulators which

† This work was supported by NSF Grant MCB-9808638, and J.V. would like to acknowledge EMBO for fellowship ALTF 509-1998.

* To whom correspondence should be addressed.

10.1021/bi000640e CCC: $19.00
Published on Web 07/21/2000

accelerate the return to the OFF-state and help to terminate the signal. Thus, elucidating the intrinsic as well as the GAP-stimulated GTPase mechanism is of great importance for understanding signal transduction and tumor formation on a molecular level. Further progress in this direction is essential for finding a way to manipulate the reaction rate of oncogenic mutants by external means.

The origin of the catalytic effect of GAP is not completely clear. In principle there are two major options: (i) the transition state of the GTPase reaction is stabilized by interaction with residues which are supplied by GAP and (ii) the interaction with GAP "pushes" Ras to a conformation which stabilizes the transition state more than the regular conformation of the isolated Ras. The first option seems to be consistent with the finding that mutations of the Arg789 residue of GAP reduce the rate constant of the Ras-GAP complex by ~2000-fold.(*8*) This indicates that the so-called "arginine-finger"(*9*) stabilizes the negatively charged transition state. The second option, which is referred to sometimes as the isomerization hypothesis (*10*−*12*), is basically an allosteric-type effect where GAP helps to preorganize Ras in a catalytic configuration. It is not clear, however, how to assess the validity of this option without translating the relevant structural information to energetics. In fact, some progress in this direction has been reported by Muegge et al. (*13*) who used the GTP-bound and the GDP bound structures of Ras before the emergence of the structure of the Ras-GAP complex, but more definitive studies with the actual structure of the complex are clearly needed.

A major progress has been made recently when the structure of the complex between the activation domain of GAP and $p21^{ras}$ (referred to as Ras-GAP) in the presence of an AlF_3 transition state (TS) analogue was solved (*8*). This was followed by the determination of the related structure of the complex of a small G-protein and its GAP (*14*).

The structural advances in the field of GTP-binding proteins and G-proteins (e.g., refs *15*−*18*) offers the unique opportunity of elucidating the detailed molecular mechanism of action of these proteins. This requires, however, some form of quantitative structure function correlation that can convert the available structural information to activation energies and therefore to the relevant rate constants and catalytic effects.

The availability of a 3-D structure for Ras and the Ras-GAP complex allows one to explore the catalytic effect of GAP using computer simulation approaches. In this paper, we will apply the empirical valence bond (EVB) method (that was used previously in studies of the "intrinsic" GTPase reaction of Ras) (*19*, *20*) to studies of the effect of GAP on the GTPase reaction of Ras. We will focus on the difference between the GTP hydrolysis reaction in the Ras-GAP complex and the isolated Ras molecule. Section II will analyze first the potential surface for the GTP hydrolysis in solution. This section will then consider the energetics of the GTPase reaction in Ras and Ras-GAP as well as some Ras mutants and use them to set up the problem of the catalytic effect of GAP. Section III will describe the method used and in particular the calibration of the EVB potential surface for GTP hydrolysis. Section IV will describe the results of the simulations for the associative and dissociative mechanism and analyze the origin of the catalytic effect of GAP.

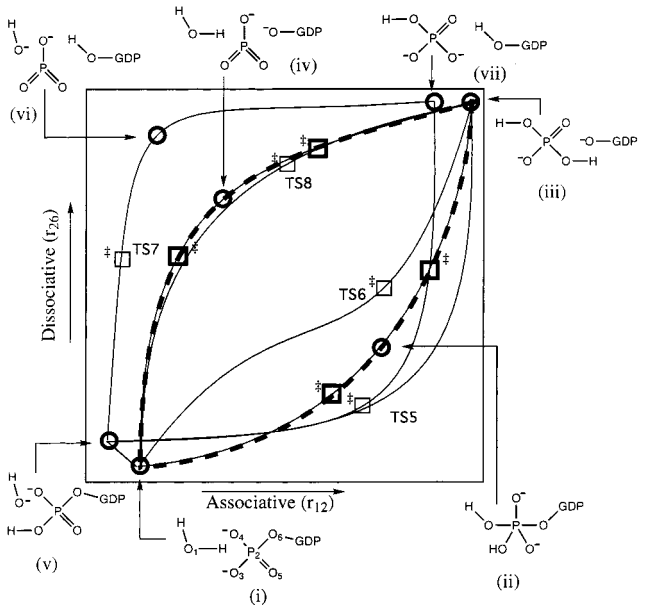

FIGURE 1: An approximated potential surface that describes the main features of the ab initio surface for the hydrolysis of monomethyl phosphate dianion. The figure considers the main path of the surface of ref *21* (light lines) and simplifies them by two "generic" pathways (black dashes) that represent the main features of the transition state region. The minima and the transition states on the surface are represented by open circles and open squares, respectively. The bold circles and squares correspond to the "generic" surface while the light circles and squares correspond to the original surface. The seven structures (states i−vii) correspond to the seven minima on the surface and the notation of the transition states (e.g., TS5) is taken from ref *21*.

GTPASE REACTION

The GTPase reaction catalyzed by Ras involves a rather complex free energy surface whose simplified nature is outlined in Figure 1. This figure focuses on the main features of the high energy plateau of the ab initio potential surface obtained by Florián and Warshel (*21*) for phosphomonoester dianions. The original surface whose main features are outlined in the figure involve several pathways that can be grouped into two classes; an associative mechanism (bottom and right path) that involves a pentacoordinated transition state (state ii) and a dissociative mechanism (top and left path) that involves the formation of a trigonal metaphosphate (state vi). Here we simplified the landscape of the ab initio surface and focus on paths that connect the seven local minima. These minima, which are designated in the figure by open circles, correspond to reactant states, intermediate states and product states. We further simplified the surface by choosing for each mechanism a single "generic" pathway (black dashes in Figure 1) that represent the main features of the corresponding mechanisms. For the associative mechanism we chose a path that moves directly from the dianion reactant state (state i) to the pentacoordinated intermediate (state ii) which is located between TS5 and TS6 [in the notation of Figure 21 of Florián and Warshel (*21*)], and finally to the product state (state iii). This path involves early and late barriers before and after the pentacoordinated intermediate. Such an approximated path is reasonable since we are mainly interested in the transition state region where the actual surface between TS5 and TS6 is very shallow and one of the main features of this surface is the availability of

late and early transition states. The possible involvement of a proton-transfer step (state i→v) is not considered explicitly since this step is not rate limiting. For the dissociative mechanism we chose a path that leads directly from the dianion reactant (state i) to the metaphosphate intermediate (state iv) and to the product (state iii). The alternative path that involves an initial proton transfer (state i→state v), formation of the intermediate vi, leading to a second product (vii) with a protonated leaving group, was not considered. Again it is assumed that the simplified pathway used represents the main features of the transition state region and the availability of early and late transition states (see also ref *22*). The experimental evidences that have been used to discriminate between the associative and dissociative paths will be considered at the end of this section.

The rate constant for the Ras catalyzed GTPase reaction is 4.7×10^{-4} s^{-1} (e.g., see ref *23*) which can be converted to an activation barrier of ~22.4 kcal/mol by applying transition state theory

$$k \cong 6 \times 10^{12} \exp[-\Delta g^{\ddagger}/RT] \qquad (1)$$

where R is the gas constant and T is the absolute temperature and the rate is given in inverse seconds (see ref *24*). The rate constant for the enzymatic reaction can be compared to the corresponding rate constant for the hydrolysis of GTP in solution. The rate constant of this solution reaction can be estimated using the relationship (*25*, *26*)

$$\log k = 0.86 - 1.23 \mathrm{p}K_a \text{ (leaving group)} \qquad (2)$$

with a pK_a of 6.4 (*27*) for the leaving group we obtain $k \approx 5.4 \times 10^{-8}$ s^{-1}. This and eq *1* give an activation barrier of 27.5 kcal/mol which should correspond to the activation barrier along the associative path of Figure 1. Thus, Ras catalyzes the corresponding solution reaction by ~5 kcal/mol. The resulting enzyme is, however, still a relatively slow enzyme with a slow conversion of GTP to GDP. The formation of the Ras-GAP complex leads to a much more efficient enzyme with a rate constant of 19 s^{-1} (*7*) and an activation barrier of ~16 kcal/mol. This large change between the activation barrier of Ras-GAP and Ras is what makes the Ras-GAP complex such an efficient switch for the signal transduction process.

Mutation experiments provide additional information about the origin of the effect of GAP on the GTPase reaction of Ras. In particular it is found (*9*) that mutations of Arg789, or the equivalent residue in a complex of Ras with NF1 (which is another GAP molecule), reduce the rate constant of the Ras-GAP complex by ~2000 so that the corresponding activation barrier is increased by ~4.5 kcal/mol. Mutations of Gln61 reduce the rate constant by an even larger factor (~2×10^{-6} s^{-1}) and increase the activation barrier by 8.5 kcal/mol (*28*). As pointed out in the introductory portion of the paper, the way by which this catalytic effect is obtained is not completely clear despite the availability of the three-dimensional structure of a transition state analogue. In particular, there remains the question as to what part of the catalytic effect is due to the interaction between the substrate and GAP and what part is due to the GAP induced conformational changes of Ras. This issue will be explored by the methods described in the next section.

Our proposal of the GTP as a base mechanism (*20*) has met a wide acceptance in the structural community (*8*, *17*, *28*−*33*), and subsequent related proposals were put forward for such systems as transducin (*28*), muscle motor ATPase myosin (*30*) and adenylyl cyclase (*17*). Furthermore, the elucidation of the structure of Ras-Ras-GAP (AlF_3) (*8*) was interpreted as an evidence for this mechanism. Yet, the idea that the general base in Ras is the phosphate itself has been challenged by some workers (*34*), who have nevertheless adopted our point that phosphate (rather than some protein group) is the acceptor of the proton of the attacking water molecules (see discussion in ref *35*). Thus, the disagreement reduces to whether the water attack involves a concerted or a stepwise mechanism and whether we have an associative or a dissociative mechanism. In examining this point it is important to consider recent works (*22*, *25*) where it has been clearly demonstrated that the arguments brought traditionally to support the dissociative mechanism could be interpreted equally well as evidence for the associative mechanism. In particular, it has been shown that the linear free energy relationships (LFERs) used to support the dissociative mechanism are equally or more consistent with an associative mechanism. Apparently the main problem with the traditional analysis was its implicit assumption of two intersecting valence bond (VB) states (a simple Marcus' type system). Such a model is in clear contrast to the actual surface deduced from ab initio studies which corresponds to three or more VB states. It is also instructive to consider at this point the arguments of Admiraal and Herschlag (*34*). These authors tried to provide experimental evidences that presumably exclude a stepwise mechanism in the attack of water on phosphate monoester monoanions, and thus excludes the phosphate as a base mechanism. It seem to us that this work merely brought back the well-known assumption (*36*−*38*) that the OH^- attack on a phosphate monoester monoanion in a stepwise mechanism is 10^9 slower than the "observed" rate. However, as was clearly established in our previous work (*39*), all the "observed" facts are rather irrelevant since they involve experiments where a methyl group substitutes the phosphate hydrogen (i.e., we have P−O−CH_3 instead of P−O−H). Unfortunately, there is no experimental way to determine the rate of OH^- attack on a phosphate monoester monoanion, since the phosphate will be deprotonated at the high pH needed to measure the kinetics of the OH^- attack. Now in the absence of experimental observations we are only left with careful ab initio studies and such calculations (e.g., ref *39*) show, in the case of phosphate monoester monoanion, that the attack of OH^- on trimethyl phosphate is indeed 10^9 slower than on methyl dihydrogen phosphate. This has invalidated the traditional assumption that studies which replace phosphate hydrogens by methyls can be used to exclude a stepwise mechanism in the unsubstituted phosphate case. Reference *34* also tried to support its assertion by considering the hydrolysis of 2,4-dinitrophenyl phosphate ($DNPP^-$) and of its diester analogue, methyl 2,4-dinitrophenyl phosphate ($MDNPP^-$) by H_2O and by F^- and other nucleophiles. It was argued that, since for these nucleophiles the ratio between the rate constants for the hydrolysis of $DNPP^-$ and $MDNPP^-$ is only between 3 and 20, it is justified to use the experimental information obtained when the phosphate hydrogen is replaced by a methyl. However, this argument is as problematic as the original argument. That

is, ref *34* basically argues that since the second step in a stepwise reaction of water with $DNPP^-$ and $MDNPP^-$ involves the attack of OH^- on DNPPH and MDNPPH, respectively, and since the overall reaction has a similar rate in both cases, the rate of the OH^- attack must be similar with or without methyl substitution. Unfortunately, this correct observation misses the fact that the OH^- attack should indeed be similar in this case. This is so since in both reactions we still have the crucial $P-O-H\cdots OH^-$ interaction which was shown to provide the major stabilization for the OH^- attack of the second step. Thus, the two compounds are expected to have similar rates of hydrolysis regardless of the substitution of one of the phosphate hydrogens by a methyl. However, it is unjustified to use experimental information obtained from studies of OH^- attack on phosphates that do not have any available P−O−H (only these cases can be studied experimentally). The kinetics of the attack of such nucleophiles as F^- is also irrelevant since here we do not have the crucial $P-O-H\cdots OH^-$ interaction. Finally, ref *34* tried to use the results from experiments with S-containing molecules but this involves the same argument used in the O-containing molecules. That is, the rate constant for OH^- attack on S-containing molecules cannot be deduced from experiments where the phosphate hydrogens are replaced by methyls; such an assumption was shown to be wrong by 10^9 in the case of the O-compounds and is expected to be similarly wrong in the case of S-containing molecules. In our opinion, in the absence of direct experimental information, it is preferable to use ab initio calculations than to invoke assumptions which are shown to be unjustified by such calculations.

The nature of the potential surface for phosphate hydrolysis in solution has been studied recently by Hu and Brinck (*40*), who considered the hydrolysis of phosphate monoester monoanion by two rather than one water molecule. This study put forward an interesting new proposal of a six-centered dissociative-type mechanism where the second water molecule participates in the chemical process and stabilizes the dissociative transition state. These workers concluded that this mechanism has a lower barrier than that of the associative mechanism. However, the inclusion of additional water molecules in the explicit quantum system is problematic since the calculations have not included the entropic penalty associated with freezing the rotation and translation of the second water molecule (which should be rather free to move around the phosphate in the ground state). Furthermore, including more and more solvent molecules explicitly in the calculation might not be fully consistent with the use of continuum solvation models. Our study of this system (*21*) considered all water molecules except the nucleophilic one as solvent molecules and estimated consistently the corresponding solute entropy and solvation free energy. This study found similar barriers for the associative and dissociative mechanisms. It is also useful to note (in contrast to the implication of ref *34*) that Hu and Brinck have not found that the GTP as a base mechanism is unlikely. That is, the study of Hu and Brinck involved a monoanion system where the dissociative mechanism is indeed a reasonable option and where an additional water molecule might form a six-centered transition state. However, this monoanion case is not directly relevant to the hydrolysis of dianions including GTP. The hydrolysis of dianion is not likely to involve six-centered transition states and the GTP hydrolysis in Ras is even less likely to involve a second reactive water (in addition to the nucleophilic water molecule). It should be clear, however, that present ab initio studies may still have errors of up to 5 kcal/mol. Also, the possible effect of explicit chemical participation of more than one water molecule should be explored, but this must be done by considering the corresponding entropic price and verifying that the approach used is capable of reproducing observed solvation energies.

In conclusion, since all the available experimental information about the reaction path from the hydrolysis of phosphate monoester dianion in solution are inconclusive (see refs *22* and *25*) we have to rely on the results of ab initio calculations and as stated above such studies (ref *21*) indicate that the barrier for the dissociative path for the GTPase reaction in solution is higher than that for the corresponding associative path.

MATERIALS AND METHODS

Simulations that determine the free energy along different feasible reaction paths, as opposed to only structures or dynamics, offer what is probably the best opportunity to accurately describe the details of enzyme catalysis (*41*). The present work performs such simulations using the EVB method coupled with an umbrella sampling/free energy perturbation (FEP) technique (*24*). The EVB method has been described numerous times (e.g., see ref *24*) and has been used extensively by our group and more recently by other research groups (e.g., refs *42*−*48*). Thus, we will cover here only the major points of relevance.

The enzyme/substrate system is divided into "quantum" and "classical" parts. The quantum part includes the portion of the substrate and the enzyme where bonds are being broken or formed. The atoms of this part are represented by a quantum mechanical Hamiltonian and are referred to as the EVB atoms. The rest of the system is described by a classical force field. The effect of the classical part on the quantum Hamiltonian is obtained through electrostatics, van der Waals, and bonding terms. The diagonal elements of the EVB Hamiltonian (the diabatic energies) describe the energies of different resonance structures of the system. These energies are represented by force field-like energy functions that reflect the intramolecular interaction between the reacting atoms in each resonance structure and the interaction between these atoms and the classical part of the system. The different resonance structures are mixed by off-diagonal elements which are represented by exponential functions. The actual ground-state surface (E_g) is obtained by diagonalizing the EVB Hamiltonian (see refs *24* and *49* for a detailed discussion). One of the main points of the EVB approach is that the EVB matrix elements are calibrated using both experimental information and/or ab initio calculations (see below and, e.g., ref *50*). This guarantees the reliability of the EVB surfaces. The EVB free energy is evaluated by driving the system from the reactant to product resonance structures. The data generated during the simulation is evaluated using a combination of the FEP and umbrella sampling approach (see ref *24* for details).

The EVB surface for the hydrolysis of GTP was constructed by fitting it to the generic ab initio-based surface of

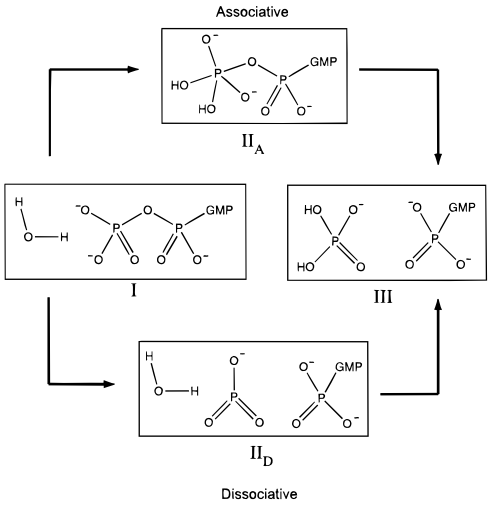

FIGURE 2: Resonance structures used in the EVB calculations for the associative mechanism (I, II_A, III) and for the dissociative mechanism (I, II_D, III).

Figure 1. This was done by choosing zero-order resonance structures whose mixing produced a potential surface similar to the generic surface. In doing so, it was required that the minima obtained by mixing the EVB resonance structures will correspond to the minima in our simplified ab initio surface. In general, the effect of the mixing is rather small at the minima and thus we force our resonance structures to have the same charge distributions and equilibrium geometries as those obtained in the corresponding ab initio calculations. At any rate, we now describe our system by the four resonance structures of Figure 2. More specifically, the potential functions for resonance structures I, II_D, and III were obtained by fitting them to the corresponding ab initio structures and charges of ref *21*. The potential function for resonance structure II_A was obtained by fitting it to the average ab initio structure and charges of TS5 and TS6 of ref *21*. The parameters used are summarized in Table 1. The table only gives relevant parameters and outline the functional forms used. The actual form of the EVB terms is given elsewhere (e.g., ref *49*).

The present work focused on the effect of GAP on the Ras reaction rather than on the catalytic effect of Ras itself. Thus, we have been concerned with the difference between the Ras-GAP potential surface and the Ras surface rather than between free energy surfaces of Ras and that of the reference solution reaction. We therefore focused on generating a qualitative surface for the associative and dissociative pathways of Ras instead of starting from the solution surface and fitting it to the surface of Figure 1. Our Ras surfaces have been assumed to retain the main features of the solution surface of Figure 1 (and ref *21*) having for each reaction path a flat transition state region with two peaks of a similar height (the square blocks in Figure 1). Although our ab initio calculations obtained a higher barrier for the dissociative path than for the associative path, we may still need a more careful determination of the actual difference between the activation barriers in solution. Thus we assumed arbitrarily that the barrier heights are similar in Ras and focused on the change of each barrier upon moving from Ras to Ras-GAP. Furthermore, we have not tried to reproduce the exact catalytic effect of Ras and in fact the calculated activation barrier is 27 kcal/mol rather than 22 kcal/mol. Better agreement could be obtained with different representation of the interaction between the Mg^{2+} ion and the phosphate oxygens but this is not the purpose of the present paper.

Table 1: Parameters Used in the EVB Calculations[a]

bond[b]	type	α	D_0	r_{ij}^0
$\Delta M(r_{ij}) = D_0[1 - e^{-\alpha(r_{ij} - r_{ij}^0)}]^2$	P−O	2.0	95.0	1.60
angle[b]	**type**	k_θ	θ_0	
$V_\theta = (k_\theta/2)\,\gamma_\theta(\theta - \theta_0)^2$	O−P−O (I,III)	50.0	109.5	
	O_{eq}−P−O_{eq} (II)	50.0	90.0	
	O_{ax}−P−O_{eq} (II)	50.0	109.5	
	O_{ax}−P−O_{ax} (II)	50.0	180.0	
	P−O−P (I,II)	50.0	120.0	
van der Waals[c]	**type**	A	B	
$V_{vdW} = A_iA_jr_{ij}^{-12} - B_iB_jr_{ij}^{-6}$	Mg	96.0	32.0	
repulsive term[d]	**type**	C	μ	
$V_{rep} = C_iC_je^{-\mu r_{ij}}$	P	30.0	2.5	
	O	35.0	2.5	
	O^-	100.0	2.5	
	H	6.0	2.5	
off-diagonal elements[e]	**type**	A_{IJ}	μ_{IJ}	
$H_{IJ} = A_{IJ}e^{-\mu_{IJ}r}$	$H_{I,II}$	65.0	0.0	
	$H_{II,III}$	40.0	0.0	
gas-phase shifts[f]	**type**	α^I		
	I	0.0		
	II	150.0		
	III	−195.0		

[a] Energies in kilocalories per mole; distances in angstroms; angles in degrees. The table lists only the parameters that are different than those used in our previous study (*19*). The table outlines the functional form of the different terms but a more complete description of the EVB terms is given elsewhere (*53*). I, II, and III designate the corresponding resonance structures. The charges of the EVB atoms are taken from ref *21*. [b] Fitted to the ab initio structures in ref *21*. [c] The interactions between the EVB atoms and the rest of the system and are represented by the standard ENZYMIX force field (*52*). [d] Repulsive nonbonded term (*57*) used for the interactions between EVB atoms. [e] The r dependent can be defined for every particular case, but note that in the present calculation the H_{ij} are taken constant. [f] The difference between the energies of the different resonance structures in the gas phase at infinite separation between the different fragments.

With the above assumption in mind, we adjusted the so-called EVB gas-phase shifts (the energies of each resonance structure at infinite separation between its fragments) and the off diagonal terms to reproduce the proper shape of the transition state region for the associative and dissociative mechanisms.

RESULTS AND DISCUSSION

Our simulation study focused on four factors: (i) the total catalytic effect of GAP in forming the Ras-GAP complex; (ii) the effect of Arg789, which was estimated by "mutating" the ionized arginine to an arginine with zero residual charge on all its atoms; (iii) the effect of Gln 61 which was estimated by mutating the charges of this residue to zero; and (iv) the effect associated with the change of the structure of Ras upon binding to GAP which was studied by simulating the reaction of Ras starting from the coordinates of Ras in Ras-GAP. This Ras model, which is designated by Ras′, was restrained to conformations which are not drastically different than the

Table 2: Activation Barriers for the Associative Mechanism of the GTPase Reaction of Ras-GAP, Ras′, and some Ras-GAP Mutants, Relative to the Corresponding Barriers in Ras[a]

enzyme	$\Delta\Delta g^{\ddagger}$	$\Delta\Delta g^{\ddagger}_{1\rightarrow 2} - \Delta G_{1\rightarrow 2}$	$\Delta g^{\ddagger}_{2\rightarrow 3}$
Set A: Position Constraint with $k = 0.3$ kcal mol^{-1} Å^{-2} for the EVB Atoms; No Mg^{2+} Constraint			
Ras	0	2	2
Ras-GAP	−7	2	0
Ras′	−10	4	1
R789NP[b] (Ras-GAP)	−4	1	0
Q61NP (Ras-GAP)	−6	8	4
Set B: Position Constraint with $k = 0.3$ kcal mol^{-1} Å^{-2} for the EVB atoms; 1 kcal mol^{-1} Å^{2} Mg^{2+} Constraint			
Ras	0	1	6
Ras-GAP	−7	4	1
Ras′	−9	8	0
R789NP (Ras-GAP)	−4	1	1
Q61NP (Ras-GAP)	−5	0	1
Set C: Position Constraint with $k = 2$ kcal mol^{-1} Å^{-2} for the EVB Atoms; No Mg^{2+} Constraints			
Ras	0	3	3
Ras-GAP	−13	2	1
Ras′	−17	4	2
R789NP (Ras-GAP)	−6	0	2
Q61NP (Ras-GAP)	−12	2	1

[a] Energies in kilocalories per mole. The activation barriers are taken relative to the corresponding barriers in Ras. $\Delta\Delta g^{\ddagger}$ is measured as the difference between the highest activation energy of Ras and the highest barrier for the other respective enzymes. $\Delta g^{\ddagger}_{1\rightarrow 2}$ and $\Delta G_{1\rightarrow 2}$ are the activation barriers and free energies for the first step. $\Delta g^{\ddagger}_{2\rightarrow 3}$ is the activation barrier for the second step. [b] NP indicates that the corresponding residue was mutated to its nonpolar form.

conformation of Ras in the Ras-GAP complex by a weak harmonic constraint, $V = 0.06\sum_i (r_i - r_i^0)^2$, where r_i^0 is the position vector of the ith atom in the X-ray structure.

We started by performing EVB calculations for the associative mechanism of Ras, Ras-GAP, and Ras′. The Ras coordinates (*51*) are those used in a previous EVB study of Ras (*20*, *51*). The Ras-GAP and Ras′ coordinates are taken from Scheffzek et al. (*8*). The EVB calculations were performed using the simulation program ENZYMIX (*52*). This involved FEP/umbrella sampling method where the system was driven from one resonance structure to another, e.g., I → II, by 11 FEP mapping steps and then using the data generated in the corresponding simulation runs in the umbrella sampling procedure. The simulations involved at least 10 ps equilibration and each of the FEP steps involved 4 ps simulation time with 1 fs time steps at 300 K. The calculations were run several times (typically four) with different initial conditions and the corresponding results were averaged. The simulations were done with three sets of structural constraints (see Table 2 and III) whose variation helped in examining the stability of the calculations (see ref *53*) for the significance of the protein, position, and distance constraints). This was done with quadratic "constraints" of the form

$$V_{\text{position}} = (k/2)\sum_i (r_i - r_i^0)^2 \qquad (3)$$

$$V_{\text{distance}} = \sum_{ij} (k_{ij}'/2)(r_{ij} - r_{ij}^0)^2 \qquad (4)$$

where r_i^0 is the X-ray position of the indicated atom and r_{ij} is the distance between the i and j atoms. Set A used $k =$ 0.3 kcal mol^{-1} Å^{-2} in constraining the positions of the EVB atoms (region I) and also applied a distance constraint with $k' = 5$ kcal mol^{-1} Å^{-2} and $r_{ij}^0 = 3$ Å for the distances between the γ-phosphorus and the attacking oxygen and for the distance between the γ-phosphorus and the leaving oxygen. These constraints helped in obtaining stable EVB results and in reducing the time needed to sample configurations at the beginning and the end of the reaction, although reducing the constraints did not change our results in a major way. Set B was designed to examine the influence of the Mg^{2+} ion. This was done by using a distance constraint with k = 1 kcal mol^{-1}Å^{-2} and $r_{ij}^0 = 2.15$ Å for the distance between the Mg^{2+} ion and carboxylic oxygen of Asp57. In addition we used the same constraints as in set A. Set C applied a position constraint with $k = 2$ kcal mol^{-1} Å^{-2} for the EVB atoms with all other constraints equal to those in set A. This set was used to examine the dependence of the calculated catalytic activity on the constraints imposed on region I atoms. The results of the simulations for the associative and dissociative paths are summarized and discussed below.

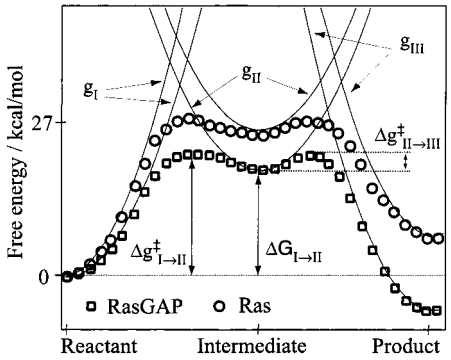

FIGURE 3: The free energy surfaces, g_I, g_{II}, and g_{III}, of the three resonance structures that describe the associative mechanism in Ras (upper solid lines) and Ras-GAP (lower solid lines) and the corresponding ground-state free energy surfaces, g, obtained from mixing the energies of the different resonance structures for Ras (circles) and Ras-GAP (squares). The calculations presented in the figure are taken from a simulation without Mg constraints.

Associative Mechanism. The results of the simulations for the associative mechanism are shown schematically in Figures 3 and Figure 4 while the corresponding data are presented in Table 2. In analyzing these results we start with the overall catalytic effect of GAP. The calculated difference between the activation free energy, $\Delta\Delta g^{\ddagger}$, of the GTPase reaction in Ras and Ras-GAP is ∼7 kcal/mol in both sets A and B. These results are in excellent agreement with the corresponding observed value of ∼6.5 kcal/mol. An insight into the nature of this catalytic effect can be obtained from Figure 3. The figure presents both the free energy functions of the indicated resonance structures and the actual ground-state free energy obtained from the mixing. As seen from this figure, the effect of GAP on the first step is manifested in the stabilization of resonance structure II (which corresponds to the pentacoordinated intermediate) and resonance structure III (which corresponds to the product state). Although the stabilization of resonance structure III is overestimated, we believe that the general trend is reasonable since it was reproduced with different simulation conditions (not all are given). A part of the stabilization effect, which will be discussed in more detail below**,** can be described as

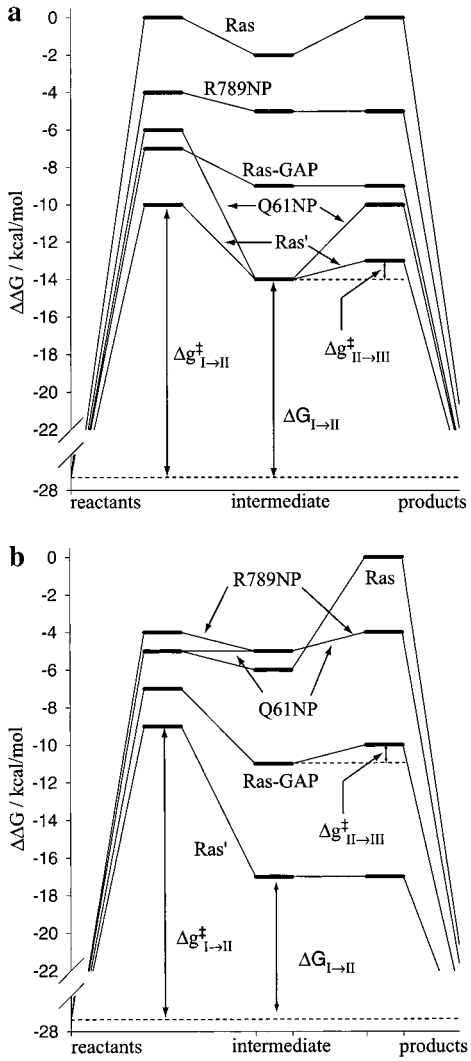

FIGURE 4: Simplified free energy diagrams for the associative mechanism with (a) no Mg constraints and (b) 1 kcal/mol Mg constraints. The figure displays the activation barriers for the first and second step as well as the free energies of the first step. The activation barriers of Ras is taken as a reference for the other systems that include Ras-GAP, Ras′, R789NP, and Q61NP where the notation NP indicates that the corresponding residue was mutated to its nonpolar form. The bars on the energy axis mark the heights of the corresponding activation barrier (relative to Ras).

the migration of a positive electrostatic potential from the γ-phosphate to the β-phosphate. In this way the formation of the Ras-GAP complex stabilizes the product (GDP) relative to the reactant (GTP), in agreement with the proposal of Muegge et al. (*13*). This electrostatic effect will be examined below.

Having reproduced the trend in the overall effect of the GAP we tried to explore the nature of different contributions to this effect. The corresponding results are summarized in Table 2 and Figure 4 which presents the relevant potential surface in a schematic way. We start by examining the effect of Arg789. The major role of this residue has been established by Wittinghofer and co-workers through both structural and mutation studies (*8*, *9*). The Arg789Ala mutation in Ras-GAP, or the equivalent mutation in the complex of Ras with NF1 (see GTPase Reaction section), results in an increase of ~4.5 kcal/mol in the activation barrier of the GTPase reaction (*9*). This effect is most likely due to a direct interaction between Arg789 and the transition state but it is still interesting to examine this issue by simulation studies. Since the effect of the Arg is largely electrostatic, we attempted to reproduce the experimental value by "mutating" the residual charges on Arg789 rather than by mutating this residue to alanine. As seen from Table 2 the catalytic effect is calculated to be 4 kcal/mol for both sets A and B, in good agreement with the experimental value.

One of the most puzzling elements of the catalytic effect of GAP is the enormous enhancement of the effect of mutations of Gln61. While mutations of Gln61 in the isolated Ras have a relatively small effect [increases of 1.5−2 kcal/mol in the activation barrier depending on the mutations (*16*, *19*)], mutations of Gln61 in the Ras-GAP complex reduce the reaction rate by up to 10^6-fold (e.g., see ref *28*) which amounts to an 8.5 kcal/mol increase in the activation barrier. This enormous effect is the reason Gln61 mutations are frequently found in tumors. The origin of this effect, however, is far from obvious. That is, Gln61 is not in a direct contact with the γ-phosphate in Ras and its proposed role as the base in a general base catalysis has been basically disproved (*19*, *35*). In the Ras-GAP complex Gln61 is pushed closer to the γ-phosphate and can in principle participate in the stabilization of the transition state (*19*, *54*). The importance or relevance of this direct interaction is, however, not well understood. To explore the catalytic effect of Gln61, we mutated its residual charges to zero in the Ras-GAP complex and evaluated the corresponding change in the activation barrier. It was found (see Table 2) that the corresponding increase in the activation barrier is rather small; 1 and 2 kcal/mol for sets A and B, respectively. These results indicate that a significant part of the catalytic effect of Gln61 may not be associated with the direct interaction between this residue and the transition state. The indirect role of Gln61 might be associated with the stabilization of a catalytic configuration of Ras (see below). This effect cannot be modeled in a simple way by direct simulations since the structure of our Gln61 mutant stayed close to that of the native Ras-GAP complex within the current simulation time. The possible use of an indirect approach to resolve this problem will be considered in the next section.

The possibility that GAP catalysis involves a significant allosteric factor was examined by comparing the activation barrier obtained with using the structure of the isolated Ras to that obtained with the structure of the Ras part of the Ras-GAP complex (Ras′) after allowing the structure to relax without the GAP part of the complex, but with the above-mentioned protein constraints. Here we find as expected that Ras′ stays near its configuration in the Ras-GAP complex, due to the constraint applied to the protein. We also find that Ras′ does not reach the configuration of Ras (within the simulation time) even in the absence of a constraint. This is due probably to the activation barrier between the two configurations. At any rate, using Ras′ we obtained a major catalytic effect; ~10 and 9 kcal/mol for sets A and B, respectively (see Table 2 and Figure 3). These results indicate that a significant part of the catalytic effect of GAP is associated with the stabilization of a catalytic configuration of Ras. In view of this finding, it is important to examine what is the origin of the effect of Ras′. First, Ras′ stabilizes the pentacoordinated intermediate more than Ras. Second, we find in agreement with the previous proposal of Muegge et al. (*13*) that Ras′ stabilizes the broken GDP-like product

more than Ras does (see below). Note that the application of the weak constraint that kept Ras′ near its initial structure is fully justified since we are interested in the effect of Ras in the configuration it has in the Ras-GAP complex. The only issue is whether the weak constraint changes the calculated catalytic effect by restricting the protein relaxation. Here we found that changing the protein constraint from 0.03 to 0.3 changes $\Delta g^{\ddagger}$ of Ras′ by only ~3 kcal/mol thus leaving our conclusion unchanged.

Since electrostatic effects play a major role in catalysis, it is instructive to examine the corresponding contributions to the catalytic effect of GAP. To do so we used the semimacroscopic version of the protein dipole langevin dipole (PDLD/S) model (*52*) and evaluated the electrostatic interactions, V_{qq}, between each protein residue to the reacting system in its reactant state, RS, and the first EVB transition state, TS1′ (obtained from the intersection of the diabatic energy surfaces corresponding to resonance structure I and II_A). The difference between $(V_{qq}^{TS})^{(i)}$ and $(V_{qq}^{RS})^{(i)}$ (where *i* designates the *i*th residue) was divided into the corresponding contributions on the γ and β phosphates in order to help in the analyses of the electrostatic effect (see below). The relevant PDLD/S results were obtained by running EVB simulations at RS and TS1′ to generate, at time intervals of 0.3 ps, six protein configurations (for each state) and then evaluating the average of the corresponding $(V_{qq}^{TS} - V_{qq}^{RS})^{(i)}$. Although this is a rather limited number of configurations it was found in previous studies (see, e.g., ref *55*) that the PDLD/S energy converges with around 10 configurations (once we start from a relaxed structure). Furthermore, the group contribution, in contrast to the effect of mutations, are a rather qualitative concept (*13*). The results of our PDLD/S analyses are depicted in Figure 5. The electrostatic contributions are presented in such a way that negative contributions of $(V_{qq}^{TS} - V_{qq}^{RS})^{(i)}$ means that the corresponding residue catalyzes the GTPase reaction in Ras-GAP or Ras′ relative to the corresponding reaction in Ras. Of course, for the GAP portion there are no corresponding residues in Ras and thus the values for Arg789 in Figure 5a reflect only the change in V_{qq} from the reactant state (resonance structure I) to the transition state. Arg789 thus stabilizes the β-phosphate by an extra ~3.5 kcal/mol relative to the ground state, in agreement with the observed effect of 4.5 kcal/mol. For the other residues, if the sum of the contributions from the γ and β phosphates is negative, then that residue can be considered to contribute to the catalytic effect through electrostatic stabilization. For example, Thr35 and Asp57 contribute to catalysis in both Ras-GAP and Ras′. According to the qualitative results of Figure 5a, the direct electrostatic contributions from Gln 61 in Ras-GAP is ~3.5 kcal/mol, which is in a reasonable agreement with the more rigorous EVB results of 1−2 kcal/mol, and is still considerably less than the 8.5 kcal/mol expected if it were directly involved in catalysis.

Figure 5 depicts, in addition to the individual contributions, the sum of these contributions for the γ and β phosphates ($\Delta V_{qq,\gamma}$, $\Delta V_{qq,\beta}$). The sum of $\Delta V_{qq,\beta}$ and $\Delta V_{qq,\gamma}$ should not be compared directly to the corresponding EVB result since the PDLD calculations involve limited averaging and since we are dealing with large opposing contributions. However, the trends in the relative contributions of the β and γ phosphate are most probably significant. The figure clearly shows that the catalytic effect of both Ras-GAP and Ras′ involves a shift of the protein positive electrostatic potential at the transition state from the γ to the β phosphate.

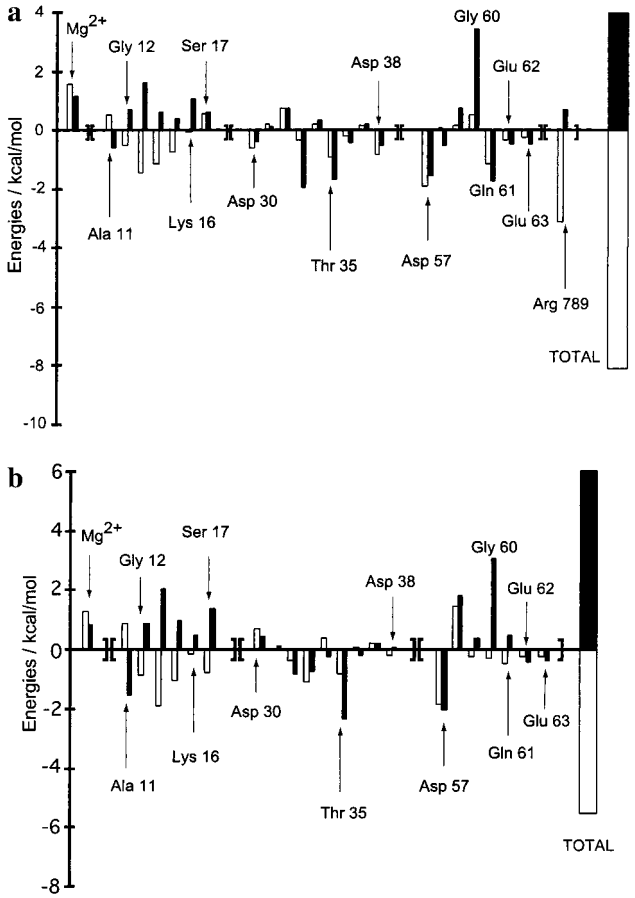

FIGURE 5: Electrostatic contributions to the catalytic effect of (a) Ras-GAP (relative to Ras) and (b) Ras′ (relative to Ras). Filled boxes represent the change in the electrostatic interaction between the given residue and the γ-phosphate to $(\Delta g^{\ddagger}_{Ras-GAP} - \Delta g^{\ddagger}_{Ras})$. Open boxes represent the change in the electrostatic interaction between the given residue and the β-phosphate to $(\Delta g^{\ddagger}_{Ras-GAP} - \Delta g^{\ddagger}_{Ras})$. Energies are given in kilocalories per mole. The box diagram on the right-hand side of the figure gives the sum of the corresponding individual contributions.

The overall trend in the change of the V_{qq} between the transition state and the reactant state is illustrated in Figure 6 for Ras, Ras-GAP, and Ras′, respectively. More specifically, the contribution on the *k*th atom is evaluated by

$$(V_{qq.k}^{TS} - V_{qq.k}^{RS}) = U_{qq.k}^{TS} Q_k^{TS} - U_{qq.k}^{RS} Q_k^{RS} \qquad (5)$$

where U_{qq} is the indicated electrostatic potential and Q_k is the atomic charge of the *k*th atom at the given state. The calculated energy contributions (the *V*s) are depicted on the atomic surface of the γ and β phosphates. The blue and red colors represent stabilizing and destabilizing contributions of V_{qq}, respectively. The degree of stabilization or destabilization is represented by the intensity of the two colors. For Ras, Figure 6a, an intense red color surrounds both the γ and β phosphates, indicating that there is a strong destabilization going from ground state to transition state (it should be kept in mind, however, that such an environmental effect will also occur in water). For Ras-GAP, however, there is an intense blue color enveloping the β-phosphate indicating

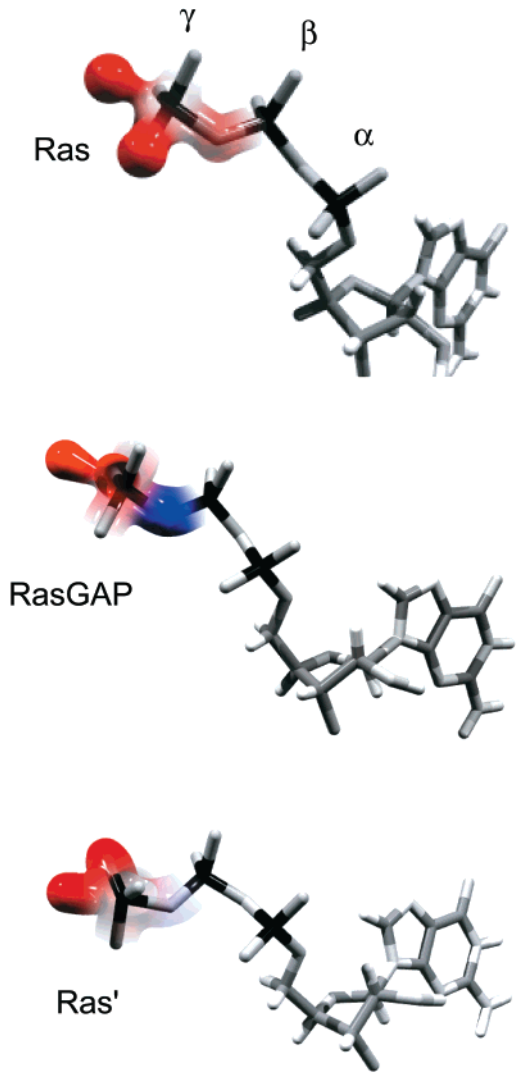

FIGURE 6: Change in electrostatic interactions, V_{qq}, between the protein residues and the γ- and β-phosphates of the substrate upon going from the reactant state to the transition state. This ΔV_{qq} is projected onto a surface around the phosphates for (a) Ras, (b) Ras-GAP, and (c) Ras′. Blue indicates a stabilizing change in V_{qq} (the difference between the transition state and the reactant state is reduced) and red a destabilizing change. The degree of stabilization or destabilization is proportional to the intensity of the color. Note that we are not presenting the change in electrostatic potential, which can be somewhat irrelevant, but rather the actual change in electrostatic energy (see eq 5).

a strong stabilization (see Figure 6b). Ras′, see Figure 6c, also provides a stabilizing energy to the β phosphate but not as strong as that provided by Ras-GAP, as depicted by the transparency of the blue color. As is clear from the figure, the location of the stabilizing V_{qq} moves toward the β phosphate upon transfer from Ras to Ras-GAP.

Dissociative Mechanism. The results for the dissociative mechanism are given in Table 3, and shown schematically in Figure 7a for the simulations with set A and in Figure 7b for the simulations with set B. Overall the trend of the results is similar to that in the associative mechanism. However, the calculated catalytic effect is overestimated. For example, Ras-GAP catalyzes the reaction of Ras by 11 and 10 kcal/mol for sets A and B as compared to the ~7 kcal/mol catalytic effect obtained with the associative model and to the observed effect of ~6.5 kcal/mol.

Table 3: Activation Barriers for the Dissociative Mechanism of the GTPase Reaction of Ras-GAP, Ras′, and Some Ras-GAP Mutants, Relative to the Corresponding Barriers in Ras[a]

enzyme	$\Delta\Delta g^{\ddagger}$	$\Delta\Delta g^{\ddagger}_{1\rightarrow2} - \Delta G_{1\rightarrow2}$	$\Delta g^{\ddagger}_{2\rightarrow3}$
Set A: Position constraint with $k = 0.3$ kcal mol^{-1} Å^{-2} for the EVB Atoms; No Mg^{+2} Constraints			
Ras	0	3	3
Ras-GAP	−13	9	2
Ras′	−11	8	0
R789NP (Ras-GAP)	−2	1	0
Q61NP (Ras-GAP)	−11	8	4
Set B: Position Constraint with $k = 0.3$ kcal mol^{-1} Å^{-2} for the EVB Atoms; 1 kcal/mol Mg^{+2} Constraints			
Ras	0	3	3
Ras-GAP	−13	7	5
Ras′	−10	11	4
R789NP (Ras-GAP)	−6	5	3
Q61NP (Ras-GAP)	−9	9	1

[a] Energies in kilocalories per mole. The activation barriers are taken relative to the corresponding barriers in Ras. $\Delta\Delta g^{\ddagger}$ is measured as the difference between the highest activation energy of Ras and the highest barrier for the other respective enzymes. $\Delta g^{\ddagger}_{1\rightarrow2}$ and $\Delta G_{1\rightarrow2}$ are the activation barriers and free energies for the first step. $\Delta g^{\ddagger}_{2\rightarrow3}$ is the activation barrier for the second step. [b] NP indicates that the corresponding residue was mutated to its nonpolar form.

The fact that the overall calculated effect of GAP and the mutations studied in this work is similar for the associative and dissociative mechanisms means that our conclusions are *independent* of the actual mechanism. It should be pointed out that the calculated activation barrier depends on the corresponding barrier for the reference reaction in water. In the present work we used for convenience the same barriers for the associative and dissociative paths in Ras. However, our studies of the hydrolysis of monomethyl phosphate dianion (see GTPase Reaction section and ref *21*) indicated that the barrier for the dissociative path is higher than that for the associative path. This would imply that the enzyme operates by using the associative path.

CONCLUDING REMARKS

The present simulation studies reproduced the overall effect of GAP on the GTPase reaction of Ras. This effect has been attributed to a combination of a direct electrostatic effect from the interaction between GAP and the transition state of the GTPase reaction and to an indirect effect due to GAP-induced structural changes of Ras. In agreement with previous studies we found that Arg789 contributes mainly by providing a direct electrostatic contribution to the transition state. On the other hand, Gln61 appeared to be involved in an indirect effect which is most probably associated with a stabilization of a catalytic configuration of Ras.

The availability of the structures of Ras in the Ras-GAP complex (the Ras′ structure) allows us to examine the possible consequences from the allosteric effect of Ras. Our calculations indicate that Ras' provides a significant effect to the GTPase reaction of Ras. This effect is associated with a shift of the positive electrostatic potential of the protein from the γ-phosphate to the $\beta-\gamma$ region. This corresponds to stabilization of the product state, the GDP bound structure, relative to the GTP bound structure. The relevant allosteric energy is distributed in a rather complex way. It involves residues in the so-called P-loop (*13*) and Asp57, and it does

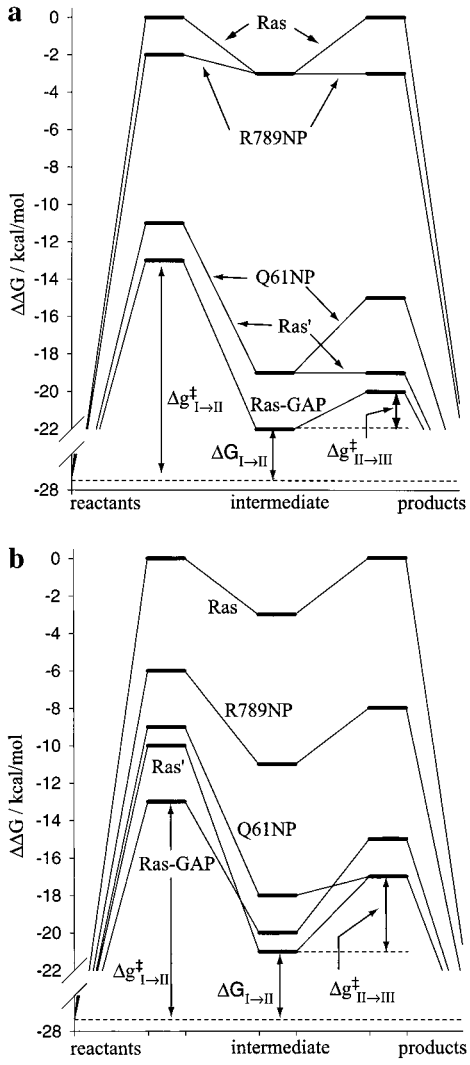

FIGURE 7: Simplified free energy diagrams for the dissociative mechanism with (a) no Mg constraints and (b) 1 kcal/mol Mg "constraints". The figure displays the activation barriers for the first and second step as well as the free energies of the first step. The activation barriers of Ras are taken as a reference for the other systems that include Ras-GAP, Ras′, R789NP, and Q61NP, where the notation NP indicates that the corresponding residue was mutated to its nonpolar form. The bars on the energy axis mark the heights of the corresponding activation barrier (relative to Ras).

not involve Glu62 and Glu63, which are close to Gln61 (see ref *13*) for a related study).

The present study examined the catalytic effect of GAP on the associative and dissociative mechanisms. It is found that the effect of GAP is similar in both cases. Thus the most likely mechanism is the one whose activation barrier is smaller in solution. Our previous ab initio study indicated that in solution the dissociative mechanism has a higher barrier than the associative mechanism. Although this is the most likely conclusion it should be instructive to examine this issue by further theoretical studies. For example, it would be instructive to find mutations whose effects on the different mechanisms is sufficiently discriminating to allow one to determine which of these mechanisms is more likely.

This work is to the best of our knowledge the first theoretical study of the catalytic effect of GAP. It should be mentioned in this respect that the recent study of ref *56* is not qualified as a realistic study of the GTPase reaction in Ras or in solution. The study of ref *56* involved gas phase ab initio calculations of a GTP molecule, two water molecules, a Mg^{2+} ion, and fragments of Thr35, Ser17, and Lys16. Such a model misses the interaction of the charged model system with its surrounding (the "solvation" energy) and thus leads to artificial results. For example, the study starts with a protonated Lys16 in the reactant state but this residue would not be protonated in the gas phase environment used in the calculations(the pK_a of Lys16 should be very low in such a model). This unstable protonated Lys thus serves as an artificial proton relay. Similarly the pK_a of the γ-phosphate must be very different than its value in its actual environment. Basically, missing the solvation of the reacting fragments by their surrounding environment prevents one from both obtaining meaningful results and from exploring the effect of the environment on these results.

linear free energy relationships (LFERs) can offer useful information on the catalytic effect of GAP and on the actual mechanism of the GTPase reaction (*35*, *54*). The difficulty is, of course, in obtaining a unique interpretation of such LFERs (*22*). Although the present study has not addressed this issue in a direct way, it is instructive to note that the present analysis involves more than two resonance structures (see Figure 2). This corresponds in many respects to the hypothetical analysis presented in ref *35*. In subsequent studies, we will try to examine the LFER predicted for the associative and dissociative mechanisms.

The role of Gln61, as well as of Gly12 and Gly13, are of particular interest in view of their high occurrence in human tumors. The present study indicates that the elusive effect of Gln61 is indirect. Thus, the focus should probably be shifted from the interaction between the residue and the transition state to the energetics of Gln61 and its mutants in the two alternative forms of the protein (Ras and Ras′). If Gln61 is more stable in the Ras′ configuration of Ras-GAP than in the Ras configuration it will shift the equilibrium toward the former and help in catalysis. Studies that attempt to determine these energetics are now underway in our lab.

ACKNOWLEDGMENT

We thank Miquel de Cáceres for providing assistance with the molecular graphics.

REFERENCES

1. Bourne, H. R., Sanders, D. A., and McCormick, F. (1991) *Nature 349*, 117−127.
2. Bourne, H. R., Sanders, D. A., and McCormick, F. (1990) *Nature 348*, 125−132.
3. Wiesmuller, L., and Wittinghofer, A. (1994) *Cell. Signaling 6*, 247−267.
4. Barbacid, M. (1987) *Annu. Rev. Biochem. 56*, 779.
5. Bos, J. (1989) *Cancer Res. 49*, 4682−4689.
6. Lowy, D. R., and Willumsen, B. M. (1993) *Annu. Rev. Biochem. 62*, 851−891.
7. Gideon, P., John, J., Frech, M., Lautwein, A., Clark, R., Scheffler, J. E., and Wittinghofer, A. (1992) *Mol. Cell. Biol. 12*, 2050−2056.
8. Scheffzek, K., Ahmadian, M. R., Kabsch, W., Wiesmuller, L., Lautwein, A., Schmitz, F., and Wittinghofer, A. (1997) *Science 277*, 333−338.
9. Ahmadian, M. R., Stege, P., Scheffzek, K., and Wittinghofer, A. (1997) *Nat. Struct. Biol. 4*, 686−689.
10. Neal, S. E., Eccleston, J. F., Hall, A., and Webb, M. R. (1988) *J. Biol. Chem. 263*, 19718−19722.
11. Moore, K. J. M., Webb, M. R., and Eccleston, J. F. (1993) *Biochemistry 32*, 7451−7459.

12. Nixon, A. E., Brune, M., Lowe, P. N., and Webb, M. R. (1995) *Biochemistry 34*, 15592−15598.
13. Muegge, I., Schweins, T., Langen, R., and Warshel, A. (1996) *Structure 4*, 475−489.
14. Rittinger, K., Walker, P. A., Eccleston, J. F., Nurmahomed, K., Owen, D., Laue, E., Gamblin, S. J., and Smerdon, S. J. (1997) *Nature 388*, 693−697.
15. Lambright, D. G., Noel, J. P., Hamm, H. E., and Sigler, P. B. (1994) *Nature 369*, 621−628.
16. Chung, H.-H., Benson, D. R., and Schultz, P. G. (1993) *Science 259*, 806−809.
17. Tesmer, J. J. G., Sunahara, R. K., Gilman, A. G., and Sprang, S. R. (1997) *Science 278*, 1907−1916.
18. Sondek, J., Bohm, A., Lambright, D. G., Hamm, H. E., and Sigler, P. B. (1996) *Nature 379*, 369.
19. Langen, R., Schweins, T., and Warshel, A. (1992) *Biochemistry 31*, 8691−8696.
20. Schweins, T., Langen, R., and Warshel, A. (1994) *Nat. Struct. Biol. 1*, 476−484.
21. Florián, J., and Warshel, A. (1998) *J. Phys. Chem. B 102*, 719−734.
22. Åqvist, J., Kolmodin, K., Florián, J., and Warshel, A. (1999) *Chem. Biol. 6*, R71−R80.
23. Temeles, G. L., Gibbs, J. B., D'Alonzo, J. S., Sigal, I. S., and Scolnick, E. M. (1985) *Nature 313*, 700−703.
24. Warshel, A. (1991) in *Computer Modeling of Chemical Reactions in Enzymes and Solutions*, John Wiley & Sons, New York.
25. Florián, J., Åqvist, J., and Warshel, A. (1998) *J. Am. Chem. Soc. 120*, 11524−11525.
26. Kirby, J. A., and Warren, S. G. (1967) *The organic chemistry of phosphorus*, Elsevier, Amsterdam.
27. Smith, R. M., and Alberty, R. A. (1956) *J. Phys. Chem. 60*, 180−184.
28. Schweins, T., Geyer, M., Scheffzek, K., Warshel, A., Kalbitzer, H. R., and Wittinghofer, A. (1995) *Nat. Struct. Biol. 2*, 36−44.
29. Sondek, J., Lambright, D. G., Noel, J. P., Hamm, H. E., and Sigler, P. B. (1994) *Nature 372*, 276−279.
30. Fisher, A. J., Smith, C. A., Thoden, J., Smith, R., Sutoh, K., Holden, H. M., and Rayment, I. (1995) *Biochemistry 34*, 8960.
31. Hansson, T., Nordlund, P., ånd Aqvist, J. (1997) *J. Mol. Biol. 265*, 118−127.
32. Thunnissen, M., Taddei, N., Ligun, G., Ramponi, G., and Nordlund, P. (1997) *Structure 5*, 69−79.
33. Dumas, J. J., Zhu, Z., Connolly, J. L., and Lambright, D. G. (1999) *Structure 7*, 413−423.
34. Admiraal, S. J., and Herschlag, D. (2000) *J. Am. Chem. Soc. 122*, 2145−2148.
35. Schweins, T., and Warshel, A. (1996) *Biochemistry 35*, 14232−14243.
36. Bunton, C. A., Llewwellyn, D. R., Oldham, K. G., and Vernon, C. A. (1958) *J. Chem. Soc.* 3574.
37. Barnard, P. W. C., Bunton, C. A., Llewellyn, D. R., Vernon, C. A., and Welch, V. A. (1961) *J. Chem. Soc.* 2670−2676.
38. Kirby, A. J., and Varvoglis, A. G. (1967) *J. Am. Chem. Soc. 89*, 415−423.
39. Florián, J., and Warshel, A. (1997) *J. Am. Chem. Soc. 119*, 5473−5474.
40. Hu, C.-H., and Brinck, T. (1999) *J. Phys. Chem. A 103*, 5379−5386.
41. Warshel, A. (1998) *J. Biol. Chem. 273*, 27035−27038.
42. Kim, H. J., and Hynes, J. T. (1992) *J. Am. Chem. Soc. 114*, 10508.
43. Grochowski, P., Lesyng, B., Bala, P., and McCammon, J. A. (1996) *Int. J. Quantum Chem. 60*, 1143−1164.
44. Neria, E., and Karplus, M. (1997) *Chem. Phys. Lett. 267*, 23−30.
45. Schmitt, U. W., and Voth, G. A. (1998) *J. Phys. Chem. B 102*, 5547−5551.
46. Kim, Y., Corchado, J. C., Villà, J., Xing, J., and Truhlar, D. G. (2000) *J. Chem. Phys. 112*, 2718−2735.
47. Lobaugh, J., and Voth, G. A. (1996) *J. Chem. Phys. 104*, 2056−2069.
48. Vuilleumier, R., and Borgis, D. (1998) *Chem. Phys. Lett. 284*, 71−77.
49. Åqvist, J., and Warshel, A. (1993) *Chem. Rev. 93*, 2523−2544.
50. Villà, J., Bentzien, J., González-Lafont, À., Lluch, J. M., Bertran, J., and Warshel, A. (2000) *J. Comput. Chem. 21*, 607−625.
51. Milburn, M., Tong, L., DeVos, A. M., Bruenger, A., Yamaizumi, Z., Nishimura, S., and Kim, S. H. (1990) *Science 247*, 939−945.
52. Lee, F. S., Chu, Z. T., and Warshel, A. (1993) *J. Comput. Chem. 14*, 161−185.
53. Glennon, T. M., and Warshel, A. (1998) *J. Am. Chem. Soc. 120*, 10234−10247.
54. Schweins, T., Geyer, M., Kalbitzer, H. R., Wittinghofer, A., and Warshel, A. (1996) *Biochemistry 35*, 14225−14231.
55. Sham, Y. Y., Chu, Z. T., and Warshel, A. (1997) *J. Phys. Chem. B 101*, 4458−4472.
56. Futatsugi, N., Hata, M., Hoshino, T., and Tsuda, M. (1999) *Biophys. J. 77*, 3287−3292.
57. Warshel, A., and Weiss, R. M. (1980) *J. Am. Chem. Soc. 102*, 6218−6226.

BI000640E